IOSR Journal of Applied Physics (IOSR-JAP)
e-ISSN: 2278-4861.Volume 18, Issue 2 Ser. II (Mar – Apr 2026), PP 09-15
www.iosrjournals.org

Structural, Thermal and Luminescent Properties of Dy^{3+} ions doped Silicate Glasses for Laser action in yellow region

S.L.Meena
Ceramic Laboratory, Department of physics, Jai Narain Vyas University, Jodhpur 342001(Raj.) India

Abstract
Glass of the system: (40-x)SiO_2: 10ZnO: 10Li_2O: 10PbO: 10Al_2O_3: 10Y_2O_3: 10Sb_2O_3:xDy_2O_3 (where x=1, 1.5,2 mol %) have been prepared by melt-quenching technique. The amorphous nature of the prepared glass samples was confirmed by X-ray diffraction. DTA curve was analysed to evaluate the glass transition temperature, crystallization temperature and melting temperature .Optical absorption and fluorescence spectra were recorded at room temperature for all glass samples. Judd-Ofelt intensity parameters Ω_λ (λ=2, 4 and 6) are evaluated from the intensities of various absorption bands of optical absorption spectra. The radiative properties like spontaneous emission probability (A), branching ratio (β), radiative life time (τ_R),stimulated emission cross–section(σ_p)and thermal properties have been evaluated.

Keywords: *YZLLAAS Glasses, Judd-Ofelt Theory, Luminescent Properties, Thermal Properties.*

I. Introduction

Glass doped with rare earth ions have several attractive spectral properties such as optical fiber amplifiers, photonic technology and infrared lasers Ceramic glass as host materials for active optical ions have attracted great interest recently due to their potential application in optical devices such as frequency-conversion materials and high transparency from near ultra violet to mid-infrared region [1-5].Among different host matrices, silicate glasses have wide range applications in the field of glass ceramics, with the advantage such as good physical and chemical stability ,low phonon energy, very high rare-earth ions solubility and low non-linear refractive index [6-9]. Silicate glasses have a best thermo-optical performance with good chemical durability, high gain and weak upconversion [10-12]. They present superior properties that include high transparency, high thermal stability, low melting point, high density and high thermal expansion coefficient. The addition of network modifier (NWF) ZnO is to improve both electrical and mechanical properties of such glasses [13-15].

The present work reports on the preparation and characterization of rare earth doped heavy metal oxide (HMO) glass systems for lasing materials. I have studied on the thermal, absorption and emission properties of Dy^{3+} doped yttrium zinc lithium lead alumino antimony silicate glasses. The intensities of the transitions for the rare earth ions have been estimated successfully using the Judd-Ofelt theory, The laser parameters such as radiative probabilities(A),branching ratio (β), radiative life time(τ_R) and stimulated emission cross section(σ_p) are evaluated using J.O.intensity parameters(Ω_λ, λ=2,4 and 6).

II. Experimental Techniques

Preparation of glasses

The following Dy^{3+}doped silicate glass samples (40-x)SiO_2: 10ZnO: 10Li_2O: 10PbO: 10Al_2O_3: 10Y_2O_3: 10Sb_2O_3:xDy_2O_3 (where x=1,1.5 and 2 mol%) have been prepared by melt-quenching method. Analytical reagent grade chemical used in the present study consist of SiO_2, ZnO, Li_2O, PbO, Al_2O_3, Y_2O_3,Sb_2O_3 and Dy_2O_3. They were thoroughly mixed by using an agate pestle mortar. then melted at 1060^0C by an electrical muffle furnace for 2h., After complete melting, the melts were quickly poured in to a preheated stainless steel mould and annealed at temperature of 350^0C for 2h to remove thermal strains and stresses. Every time fine powder of cerium oxide was used for polishing the samples. The glass samples so prepared were of good optical quality and were transparent. The chemical compositions of the glasses with the name of samples are summarized in **Table 1.**

Table 1.

Chemical composition of the glasses

Sample	**Glass composition (mol %)**
YZLLAAS (UD)	**40SiO_2: 10ZnO: 10Li_2O: 10PbO: 10Al_2O_3: 10Y_2O_3: 10Sb_2O_3**
YZLLAAS DY (1.0)	**39SiO_2: 10ZnO: 10Li_2O: 10PbO: 10Al_2O_3: 10Y_2O_3: 10Sb_2O_3: 1 Dy_2O_3.**
YZLLAAS DY (1.5)	**38.5SiO_2: 10ZnO: 10Li_2O: 10PbO: 10Al_2O_3: 10Y_2O_3: 10Sb_2O_3:1.5 Dy_2O_3.**
YZLLAAS DY (2.0)	**38SiO_2: 10ZnO: 10Li_2O: 10PbO: 10Al_2O_3: 10Y_2O_3: 10Sb_2O_3:2Dy_2O_3.**

YZLLAAS (UD) -Represents undoped Yttrium Zinc Lithium Lead Alumino Antimony Silicate glass specimens.
YZLLAAS (DY) -Represents Dy^{3+} doped Yttrium Zinc Lithium Lead Alumino Antimony Silicate glass specimens.

III.Theory

3.1 Oscillator Strength

The intensity of spectral lines are expressed in terms of oscillator strengths using the relation [16].

$$f_{expt.} = 4.318 \times 10^{-9} \int \varepsilon(\nu)\, d\nu \qquad (1)$$

where, $\varepsilon(\nu)$ is molar absorption coefficient at a given energy ν (cm^{-1}), to be evaluated from Beer–Lambert law. Under Gaussian Approximation, using Beer–Lambert law, the observed oscillator strengths of the absorption bands have been experimentally calculated [17], using the modified relation:

$$P_m = 4.6 \times 10^{-9} \times \frac{1}{cl} \log \frac{I_0}{I} \times \Delta\upsilon_{1/2} \qquad (2)$$

where c is the molar concentration of the absorbing ion per unit volume, I is the optical path length, $\log I_0/I$ is optical density and $\Delta\upsilon_{1/2}$ is half band width.

3.2. Judd-Ofelt Intensity Parameters

According to Judd [18] and Ofelt [19] theory, independently derived expression for the oscillator strength of the induced forced electric dipole transitions between an initial J manifold $|4f^N (S, L) J\rangle$ level and the terminal J' manifold $|4f^N (S', L') J'\rangle$ is given by:

$$\frac{8\Pi^2 mc\bar{\upsilon}}{3h(2J+1)} \frac{1}{n}\left[\frac{(n^2+2)^2}{9}\right] \times S(J, J') \qquad (3)$$

Where, the line strength S (J, J') is given by the equation

$$S(J, J') = e^2 \sum_{\lambda=2,4,6} \Omega_\lambda \langle 4f^N (S, L) J \| U^{(\lambda)} \| 4f^N (S', L') J' \rangle^2 \qquad (4)$$

In the above equation m is the mass of an electron, c is the velocity of light, ν is the wave number of the transition, h is Planck's constant, n is the refractive index, J and J' are the total angular momentum of the initial and final level respectively, Ω_λ (λ=2,4and 6) are known as Judd-Ofelt intensity parameters .

3.3 Radiative Properties

The Ω_λ parameters obtained using the absorption spectral results have been used to predict radiative properties such as spontaneous emission probability (A) and radiative life time (τ_R), and laser parameters like fluorescence branching ratio (β_R) and stimulated emission cross section (σ_p).

The spontaneous emission probability from initial manifold $|4f^N (S', L') J'\rangle$ to a final manifold $|4f^N (S, L) J\rangle$ is given by:

$$A[(S', L') J'; (S, L) J] = \frac{64\pi^2\nu^3}{3h(2J'+1)}\left[\frac{n(n^2+2)^2}{9}\right] \times S(J', \bar{J}) \qquad (5)$$

Where, $S(J', J) = e^2 [\Omega_2 \| U^{(2)} \|^2 + \Omega_4 \| U^{(4)} \|^2 + \Omega_6 \| U^{(6)} \|^2]$

The fluorescence branching ratio for the transitions originating from a specific initial manifold $|4f^N (S', L') J'\rangle$ to a final many fold $|4f^N (S, L) J\rangle$ is given by

$$\beta\,[(S', L')\,J'; (S, L)\,J] = \sum_{S\,L\,J} \frac{A[(S'\ L)]}{A[(S'\ L')\,J'(\bar{S}\ \bar{L})]} \qquad (6)$$

where, the sum is over all terminal manifolds.
The radiative life time is given by

$$\tau_{rad} = \sum_{S\,L\,J} A[(S', L')\,J'; (S, L)] = A_{Total}^{-1} \qquad (7)$$

where, the sum is over all possible terminal manifolds. The stimulated emission cross -section for a transition from an initial manifold $|4f^N (S', L')\,J'>$ to a final manifold $|4f^N (S, L)\,J>|$ is expressed as

$$\sigma_p(\lambda_p) = \left[\frac{\lambda_p^4}{8\pi c n^2 \Delta\lambda_{eff}}\right] \times A[(S', L')\,J'; (\bar{S}, \bar{L})\bar{J}] \qquad (8)$$

where, λ_p the peak fluorescence wavelength of the emission band and $\Delta\lambda_{eff}$ is the effective fluorescence line width.

IV. Result and Discussion

4.1 XRD Measurement

Figure 1 presents the XRD pattern of the sample contain – SiO_2 which is show no sharp Bragg's peak, but only a broad diffuse hump around low angle region. This is the clear indication of amorphous nature within the resolution limit of XRD instrument.

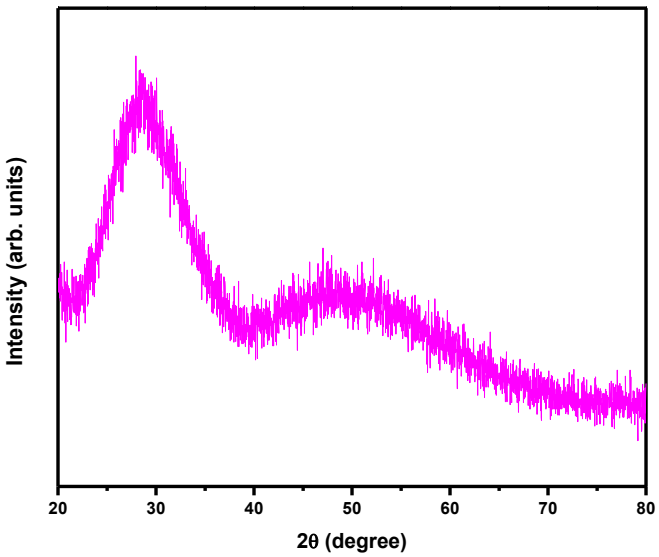

Fig. 1 X-ray diffraction pattern of SiO_2: ZnO: Li_2O: PbO: Al_2O_3: Y_2O_3: Sb_2O_3:Dy_2O_3.

4.2 Thermal Property

Differential thermal analysis checks the heat absorbed by glass samples during heating or cooling. Fig. 2 depicts the DTA thermogram of powdered YZLLAAS sample. The glass transition temperature (T_g), onset crystallization temperature (T_c), crystallization temperature (T_p), melting temperature(T_m), thermal stability (T_s),Balaji Parameter (B_P), Hurbe's criterion (H_R) and reduced glass transition temperature (T_{rg}) were calculated. Shankar's parameter also calculated by using eq. (13). All the determined thermal parameters are given in table 2.

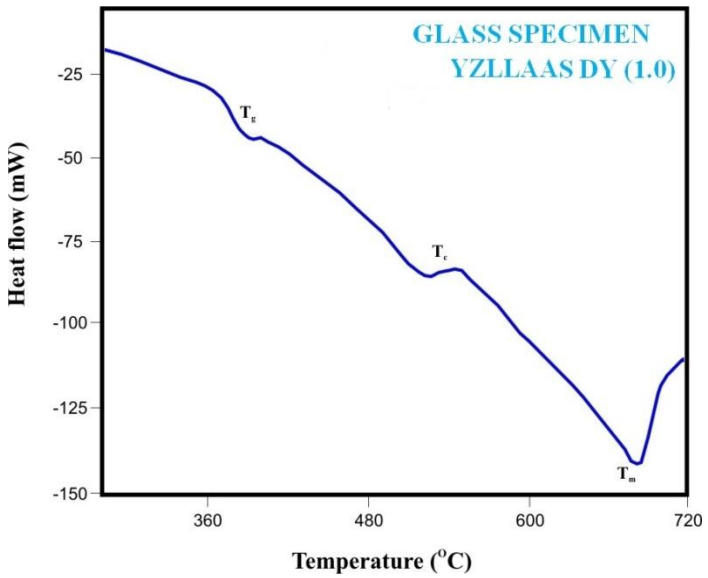

Fig.2: DTA curve of YZLLAAS DY (1.0) glass.

Table 2. Thermal parameters determined from the DTA traces of YZLLAAS DY glasses.

Sample Name	T_g (^{0}C)	T_c(^{0}C)	T_p(^{0}C)	T_m(^{0}C)	T_s(^{0}C)	B_P(^{0}C)	H_R(^{0}C)	K_S(^{0}C)	T_{rg}(^{0}C)
YZLLAAS DY (1.0)	375	510	548	685	135	3.553	0.217	34.489	0.547
YZLLAAS DY (1.5)	381	511	550	687	130	3.333	0.222	33.304	0.555
YZLLAAS DY (2.0)	385	513	555	693	128	2.048	0.223	33.724	0.556

The thermal stability of the glass samples can be calculated by difference between onset crystallization temperature and transition temperature [20].

Thermal Stability (T_s)= T_c-T_g (9)

Balaji Parameter can be calculated using [20].

Balaji Parameter (B_P) = [(T_c-T_g)/(T_p-T_c)] (10)

Hruby's criterion is calculated using the Hurby's relation [20].

Hruby'scriterion(H_R)=[(T_p-T_c)/(T_m-T_c)] (11)

Reduced glass transition temperature is given as [20].

Reduced glass transition temperature (T_{rg}) =T_g/T_m (12)

Thermal Parameter is given as [20].

K_S= [(T_m-T_c) (T_c-T_g)/T_m] (13)

4.3 Absorption Spectrum

The absorption spectra of Dy^{3+}doped YZLLAAS glass specimens have been presented in Figure 3 in terms of Intensity versus wavelength. Thirteen absorption bands have been observed from the ground state $^6H_{15/2}$ to excited states $^6H_{13/2}$, $^6H_{11/2}$, $^6H_{9/2}$+$^6F_{11/2}$,$^6H_{7/2}$+$^6F_{9/2}$,$^6F_{7/2}$+$^6H_{5/2}$,$^6F_{5/2}$,$^6F_{3/2}$,$^6F_{9/2}$,$^4I_{15/2}$,$^4G_{11/2}$, $^6F_{7/2}$+$^4I_{13/2}$, $^6M_{19/2}$+4(P,D)$_{3/2}$ and $^4G_{9/2}$+$^6P_{3/2}$ for Dy^{3+}doped YZLLAAS glasses.

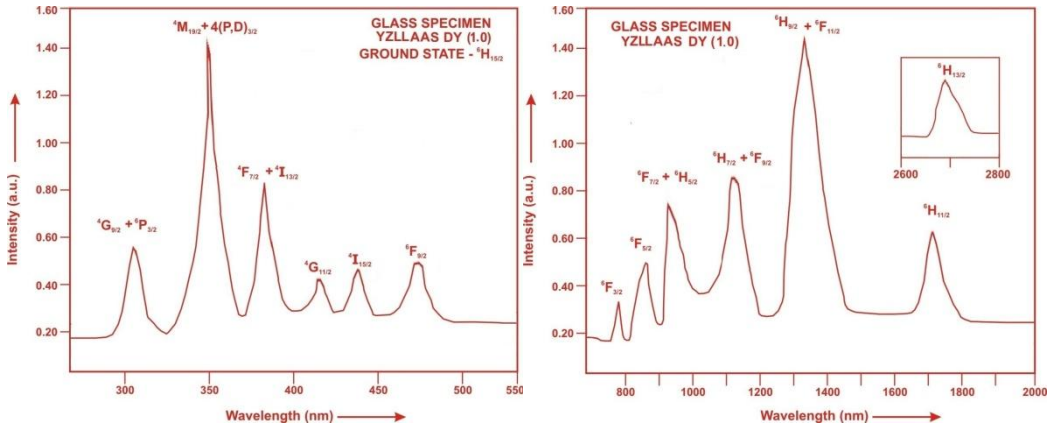

Fig. (3) Absorption spectrum of YZLLAAS DY(1.0) glass.

The experimental and calculated oscillator strength for Dy^{3+} ions in YZLLAAS glasses are given in **Table 3.**

Table 3: Measured and calculated oscillator strength ($P_m \times 10^{+6}$) of Dy^{3++}ions in YZLLAAS glasses.

Energy level from $^6H_{15/2}$	**Glass YZLLAAS DY(1.0)**		**Glass YZLLAAS DY(1.5)**		**Glass YZLLAAS DY(2.0)**	
	$P_{exp.}$	$P_{cal.}$	$P_{exp.}$	$P_{cal.}$	$P_{exp.}$	$P_{cal.}$
$^6H_{13/2}$	3.55	3.17	3.52	3.16	3.49	3.14
$^6H_{11/2}$	2.75	3.22	2.73	3.20	2.69	3.17
$^6H_{9/2}$+$^6F_{11/2}$	11.92	12.01	11.90	11.98	11.86	11.94
$^6H_{7/2}$+$^6F_{9/2}$	6.98	6.75	6.95	6.72	6.93	6.70
$^6F_{7/2}$+$^6H_{5/2}$	5.99	5.89	5.96	5.89	5.93	5.81
$^6F_{5/2}$	2.92	2.96	2.90	2.93	2.86	2.91
$^6F_{3/2}$	1.09	0.56	1.07	0.55	1.05	0.55
$^6F_{9/2}$	1.12	0.45	1.09	0.45	1.07	0.45
$^4I_{15/2}$	1.15	1.15	1.13	1.14	1.10	1.13
$^4G_{11/2}$	0.99	0.14	0.96	0.14	0.94	0.14
$^6F_{7/2}$+$^4I_{13/2}$	4.90	5.20	4.86	5.18	4.82	5.14
$^6M_{19/2}$+4(P,D)3/2	8.99	10.55	8.96	10.53	8.93	10.55
$^4G_{9/2}$+$^6P_{3/2}$	2.82	3.16	2.79	3.14	2.75	3.12
r.m.s. deviation	0.5906		0.5860		0.5937	

The values of Judd-Ofelt intensity parameters are given in **Table 4.**

Table 4: Judd-Ofelt intensity parameters for Dy^{3+} doped YZLLAAS glass specimens

Glass Specimen	**Ω_2(pm^2)**	**Ω_4(pm^2)**	**Ω_6(pm^2)**	**Ω_4 /Ω_6**	**Ω_λ Tendency**	**Ref.**
YZLLAAS DY(1.0)	3.683	1.313	2.508	0.5235	**$\Omega_2 > \Omega_6 > \Omega_4$**	P.W.
YZLLAAS DY(1.5)	3.673	1.315	2.488	0.5285	**$\Omega_2 > \Omega_6 > \Omega_4$**	P.W.
YZLLAAS DY(2.0)	3.646	1.331	2.462	0.5406	**$\Omega_2 > \Omega_6 > \Omega_4$**	P.W.
YZLCBBB (TB)	8.037	2.190	2.819	0.7769	**$\Omega_2 > \Omega_6 > \Omega_4$**	[21]
PSWB (ND)	7.590	4.117	5.543	0.7427	**$\Omega_2 > \Omega_6 > \Omega_4$**	[22]
BSPAKBL(ND)	4.388	2.998	3.676	0.816	**$\Omega_2 > \Omega_6 > \Omega_4$**	[23]
BG(ER)	6.838	1.185	2.888	0.410	**$\Omega_2 > \Omega_6 > \Omega_4$**	[24]
PZ(ND)	5.460	3.220	4.290	0.751	**$\Omega_2 > \Omega_6 > \Omega_4$**	[25]

4.4 Excitation Spectrum

The Excitation spectra of Dy^{3+}doped YZLLAAS glass specimens have been presented in Figure 4 in terms of Excitation Intensity versus wavelength. The excitation spectrum was recorded in the spectral region 315–465 nm fluorescence at 575nm having different excitation band centered at 321,354, 365, 385, 425, 455 and 473 nm are attributed to the $^6P_{3/2}$, $^6P_{7/2}$, $^4P_{3/2}$, $^4I_{13/2}$, $^4G_{11/2}$, $^4I_{15/2}$ and $^4F_{9/2}$ transitions, respectively. The highest absorption level is $^4I_{13/2}$ and is at 385nm.So this is to be chosen for excitation wavelength.

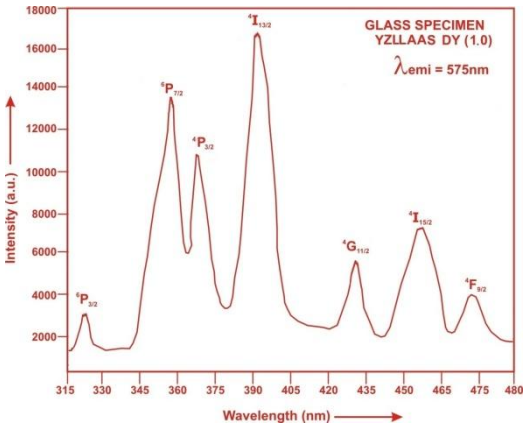

Fig. (4) Excitation spectrum of YZLLAAS DY(1.0) glass.

4.5. Fluorescence Spectrum

The fluorescence spectrum of Dy^{3+}doped in Yttrium Zinc Lithium Lead Alumino Antimony Silicate glass is shown in Figure 5. There are three broad bands observed in the Fluorescence spectrum of Dy^{3+}doped Yttrium Zinc Lithium Lead Alumino Antimony Silicate glass. The wavelengths of these bands along with their assignments are given in Table 5. The peak with maximum emission intensity appears at 485nm, 575 nm and 665 nm and corresponds to the ($^4F_{9/2}\rightarrow{}^6H_{15/2}$), ($^4F_{9/2}\rightarrow{}^6H_{13/2}$) and ($^4F_{9/2}\rightarrow{}^6H_{11/2}$) transition.

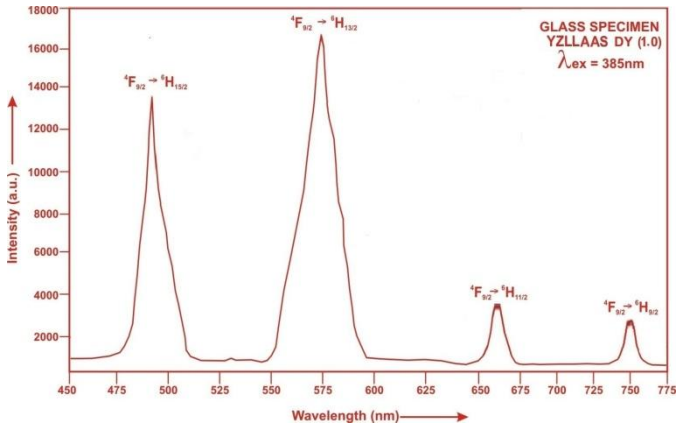

Fig. (5). Fluorescence spectrum of YZLLAAS DY(1.0) glass.

Table5: Emission peak wave lengths (λ_p),radiative transition probability (A_{rad}),branching ratio (β),stimulated emission cross-section(σ_p) and radiative life time(τ_R) for various transitions in Dy^{3+} doped YZLLAAS glasses.

Transition		YZLLAAS DY(1.0)				YZLLAAS DY (1.5)				YZLLAAS DY (2.0)			
	λ_{max} (nm)	$A_{rad}(s^{-1})$	β	σ_p (10^{-20} cm^2)	τ_R(μs)	$A_{rad}(s^{-1})$	β	σ_p (10^{-20} cm^2)	τ_R (μs)	$A_{rad}(s^{-1})$	β	σ_p (10^{-20} cm^2)	τ_R (10^{-20} cm^2)
$^4F_{9/2}\rightarrow{}^6H_{15/2}$	485	127.40	0.2250	0.223	1766.03	126.73	0.2245	0.217	1771.46	125.88	0.2242	0.213	1781.27
$^4F_{9/2}\rightarrow{}^6H_{13/2}$	575	373.30	0.6593	1.352		372.38	0.6596	1.320		370.34	0.6597	1.278	
$^4F_{9/2}\rightarrow{}^6H_{11/2}$	665	37.32	0.0659	0.166		37.26	0.0660	0.1637		37.08	0.0661	0.0160	
$^4F_{9/2}\rightarrow{}^6H_{9/2}$	752	28.23	0.0498	0.172		28.18	0.0499	0.1691		28.09	0.0500	0.0166	

V. Conclusion

In the present study, the glass samples of composition (40-x)SiO_2: 10ZnO: 10Li_2O: 10PbO: 10Al_2O_3: 10Y_2O_3: 10Sb_2O_3:xDy_2O_3, (where x =1, 1.5and 2mol %) have been prepared by melt-quenching method. The value of stimulated emission cross-section (σ_p) is found to be maximum for the transition ($^4F_{9/2}\rightarrow{}^6H_{13/2}$) for all glass specimens. This shows that ($^4F_{9/2}\rightarrow{}^6H_{13/2}$) transition is most probable transition. The high values of Balaji parameter indicate the delay in nucleation activity.

References:

[1]. Meena, S.L.(2025).Spectroscopic and Photoluminescence properties of Ho^{3+} doped borate glasses with NIR light emission applications,IOSR,Appl.Phys.17,34-40.

[2]. Matos,I.R.M.(2023).Influence of alkali metal ions on the structural and spectroscopic properties of Sm^{3+} doped silicate glasses,Ceram.6,1788-1798.

[3]. Dousti, M.R. , Poirier, G.Y., de Camargo, A.S.S.(2020).Tungsten Sodium Phosphate glasses doped with trivalent rare earth ions (Eu^{3+}, Tb^{3+}, Nd^{3+}, Er^{3+}) for visible and near infrared applications. Journal of Non- Crystalline Solids 530, 119838.

[4]. Kemere,M.,Sperga,J.,Rogulis,U.,Krieke,G.,Grube,J.(2017).Structural and optical studies on Sm^{3+} ions doped bismuth fluoroborate glasses for visible laser applications,J.Lumin.181,25-30.

[5]. Meena, S.L.(2018).Spectral and Thermal properties of Tb^{3+} doped in lead lithium borophosphate glasses,Int.Cem.Phys.Sci.7,1-8.

[6]. Babu,K.V.,Cole,S.(2018).Luminescence properties of Dy^{3+} doped alkali lead alumino borosilicate glasses,Ceram.Int.9080-9090.

[7]. Cao,W.,Huang,F.,Wang,T.,Ye,R.,Lei,R.,Tian,Y.,Zhang,J.,Xu,S.(2018).2.0μm emission of Ho^{3+} doped germanosilicate glass sensitized by non-rare earth ion Bi: a new choice for 2.0 μm laser,Opt.Mater,75,695-698.

[8]. Monisha, M., Nancy,A. , Souza, D., Nimitha ,V. L., Prabhu, S and Sayyed, M.I.(2020). Dy^{3+} doped SiO_2- B_2O_3-Al_2O_3-NaF-ZnF_2 glasses: An exploration of optical and gamma radiation shielding features, Current Applied Physics 20(11), 1207-1210.

[9]. Rao,T.G.V.M., Kumar, A. R., Neeraja, K., Veeraiah, N.and Reddy, M.R.(2013).Optical and structural investigation of Eu^{3+} ions in Nd^{3+} co-doped magnesium lead borosilicate glasses, J. Alloy. Compd. 557,209–217.

[10]. Matos,I.M.,Balzaretti,N.M.(2024).Effect of mixed alkali ions on the structural and spectroscopic properties of Nd^{3+} doped silicate glasses,Res.Mat.21,100517.

[11]. Cicconi,M.R.,Deng,H.,Otsuka,T.,Telakula Mahesh,A., Khansur,N.H., Hayakawa,T., de Light,D. (2024). Photoluminescence study of undoped and Eu-doped Alkali-Niobate Aluminosilicate Glasses and Glass-Ceramics,Mat.17,2283.

[12]. Sroda,M.,Swiontek,S.,Gieszczyk,W.,Bilski,P.(2020).The effect of lithium fluoride on the thermal stability and thermoluminescence properties of borosilicate glass and glass ceramics,J.Eur,Ceram.Soc.40,472-479.

[13]. Mi-tang Wang , Jin-shu Cheng, Mei Li and Feng He(2011). Structure and properties of soda lime silicate glass doped with rare earth. Physica B 406, 187–191.

[14]. Kilic,G.,Ilik,E.,Mahmoud,K.A.,Mallawany,R.El,Agawany,El(2020).Novel zinc vanadyl borophosphate glasses:ZnO-V_2O_5-P_2O_5-B_2O_3:Physical,thermal and nuclear radiation shielding properties,Ceram.Int.46,19318-19327.

[15]. Meena,S.L.(2021).Spectral and Raman Analysis of Sm^{3+} doped in Zinc Lithium Sodalime Alumino Silicate Glasses,Int.J.Eng.Sci.Inven.10,28-33.

[16]. Meena,S.L.(2025).Spectral and Photoluminescence Properties of Nd^{3+} doped Borotellurite Glasses for 1.08μm photonic devices,, IOSR Appl.Phys.17,41-47.

[17]. Meena,S.L.(2021). Spectral and Raman Analysis of Er^{3+} doped Zinc Lithium Antimony Sodalime Tellurite Glasses, Int.J.Eng.Sci.Inv.10, 09-15.

[18]. Judd, B.R. (1962). Optical Absorption Intensities of Rare Earth Ions. Physical Review, 127, 750.

[19]. Ofelt, G.S. (1962). Intensities of Crystal Spectra of Rare Earth Ions. The J. Chem. Phys., 37, 511. [20].Meena,S.L.(2026). Structural, Thermal and Photoluminescence analysis of Pr^{3+} doped borophosphate glasses for the visible light emitting diodes applications, IOSR Appl.Phys.18,55-62.

[20]. Meena, S.L.(2025).Spectral and Raman Analysis of Tb^{3+} doped Yttrium Zinc Lithium Cesium Barium Bismuth Borate Glasses, IOSR Appl.Phys.17,41-47.

[21]. Prasad,R.N.A.,Siva,B.V.,Neeraja,K.,Mohan,N.K.,Rojas,J.I.(2020).Influence of modifier on spectroscopic features of Nd^{3+} doped PbO-Ro_2O_3-WO_3-B_2O_3 glasses(with Ro_2O_3=Sb_2O_3,Al_2O_3 and Bi_2O_3),J.Lumin.223,117171,1-8.

[22]. Kozhanov,V.O.,Zaderko,A.N.,Boldyrieva,O.Y.,Lisnyak,V.L.(2016).Judd-Ofelt analysis of Nd^{3+} doped phosphate glass: The effect of Ba/Sr ratio,Mol.Cryst.Liq.Cryst.639,78-86.

[23]. Kashif,I.,Ratep,A.(2023).Luminescence in Er^{3+} co-doped bismuth germinate glass-ceramics for blue and green emitting applications,J.Kor.Ceram.Soc.60,511-526.

[24]. Mahraz,Z.A.S.,Sazali,E.S.,Sahar,M.R.,Anuran,N.U.,Yaacob,S.N.S.,Aziz,S.M.,Mawlud,S.Q.,Noor,F.M.,Harum,A.N.(2019).Spectroscopic investigations of near infrared emission from Nd^{3+} doped zinc phosphate glasses,Judd-Ofelt evaluation,J.Non-Cryst.Solids,509,106-114.